

Water Mass Structure of Warm and Cold Anticyclonic Eddies in the Western Boundary Region of the Subarctic North Pacific

SACHIHIKO ITOH AND ICHIRO YASUDA

Atmosphere and Ocean Research Institute, The University of Tokyo, Kashiwa, Japan

(Manuscript received 1 April 2010, in final form 29 July 2010)

ABSTRACT

Vertical profile data of temperature and salinity from various sources were analyzed together with satellite altimeter data to investigate the water mass characteristics of warm and cold anticyclonic eddies in the western boundary region of the subarctic North Pacific. A dense distribution of anticyclonic eddies with warm and saline core water occurred near the Kuroshio Extension, and the distribution extends northward–northeastward into the western subarctic gyre along the Japan and Kuril–Kamchatka trenches. Eddies with cold and fresh core water are found mainly around the Oyashio southward intrusions and farther north near the Kuril Islands. Based on the heat content anomaly integrated over 50–200 dbar, 85% of the anticyclonic eddies within the study area (35°–50°N, 140°–155°E) have a warm and saline core and 15% have a cold and fresh core. Warm and saline eddies around the Japan and Kuril–Kamchatka trenches have a double-core structure, with a cold and freshwater mass located below the warm core. The northward propagation of these eddies along the trench line results in a large northward heat (salinity) transport in the upper 400 dbar (250 dbar) and a negative salinity transport below 350 dbar. The lower core water is colder and fresher on isopycnal surfaces at around $26.70\sigma_\theta$ compared with the climatology. Given that the $26.70\sigma_\theta$ isopycnal surface does not outcrop in the open North Pacific, an alignment process is suggested to occur between the warm and saline and the cold and fresh anticyclonic eddies in the upper and intermediate layers, respectively.

1. Introduction

Intense mesoscale eddies are characterized by the nature of the water mass in their core, and the persistence of such eddies has a strong influence on the local hydrography and ecology. Some such eddies, including those from the Kuroshio Extension (KE) and the Agulhas Retroflexion, propagate to regions far from their formation sites and are considered to play important roles in intergyre or interocean exchanges of heat, materials, and biota (Gordon 1985; Itoh and Yasuda 2010, hereafter IY10).

Under the significant influence of the Coriolis force, high (low) pressure occurs at the center of anticyclonic (cyclonic) eddies. For surface-intensified eddies, this high (low) pressure at their center corresponds to a surface elevation (depression) and to horizontally less dense (denser) core water in the upper layer. In many cases, the less dense (dense) core water is caused by high

(low) temperatures, and the term “warm-core ring” (“cold-core ring”) is commonly used to indicate isolated and strongly nonlinear anticyclonic (cyclonic) eddies with a long lifetime (Olson 1991).

Anticyclonic warm-core rings are formed from western boundary currents of subtropical gyres and their extension currents, such as the Kuroshio Extension (Yasuda et al. 1992, hereafter Y92), the East Australian Current in the Tasman Sea (Nilsson and Cresswell 1980), the Gulf Stream east of the Gulf of Mexico (Elliott 1982) and east of Cape Hatteras (Richardson 1983), the Brazil Current at the Brazil–Malvinas confluence (Olson et al. 1988), and the Agulhas Retroflexion (Gordon 1985; Byrne et al. 1995). These warm-core rings generally contain warm and saline water that originated from a subtropical gyre, and their properties show a gradual change when located in relatively cold and fresh ambient water as well as cooling in winter (Olson et al. 1992; Y92). In some of the above regions, cyclonic eddies with cold and freshwater are observed to pinch off into a subtropical gyre (Ring Group 1981; Qiu et al. 2006).

In the western boundary region of the subarctic North Pacific, anticyclonic eddies with cold and fresh cores

Corresponding author address: Sachihiko Itoh, Atmosphere and Ocean Research Institute, The University of Tokyo, 5-1-5 Kashiwanoha, Kashiwa, Chiba 277-8564, Japan.
E-mail: itohsach@ori.u-tokyo.ac.jp

have been reported since the early 1990s (Lobanov and Bulatov 1993). The detailed structure of these eddies has been described by Yasuda et al. (2000, hereafter Y00) and Rogachev (2000). In the area southeast of Bussol' Strait in the Kuril Straits, cold ($<3^{\circ}\text{C}$), fresh (<33.5 psu), and low-potential-vorticity water is commonly found in the core of anticyclonic eddies in the upper layer, typically in the potential density range of 26.70–26.80 (Y00). Y00 recognized two types of eddies based on core temperature: very cold ($<2^{\circ}\text{C}$) and moderately cold (those eddies with little water $<2^{\circ}\text{C}$). The authors suggested two processes for the formation of cold-core anticyclonic eddies: direct formation from the low-potential-vorticity, cold, freshwater outflow from the Sea of Okhotsk and modification of warm-core rings that originate from the Kuroshio Extension. Although the second process is unique to the study area, observational data reveal that intense anticyclonic warm-core rings that are shed from the Kuroshio Extension tend to move northward over a period of several years, approximately following the Japan Trench (JT) and the Kuril–Kamchatka Trench (KKT; see Fig. 1; Y92).

However, the above processes have yet to be confirmed because previous observations in the present study region were limited to coastal areas on just a small number of occasions. Given that cold-core anticyclonic eddies also occur in areas farther south, around the coastal intrusion of the Oyashio Current (OY; this intrusion denoted as OY1 in Fig. 1; Shimizu et al. 2001), where a large number of warm-core rings occur (Kitano 1975), it is necessary to examine the distribution and structure of both warm-core and cold-core anticyclonic eddies with a wide spatial coverage and on repeated occasions.

Recently, IY10 quantified the distribution, intensity, and propagation speed of mesoscale eddies in the Kuroshio–Oyashio extension region, using sea surface height anomaly (SSHA) maps derived from satellite altimetry data. They found that strong anticyclonic eddies detach from the Kuroshio Extension and propagate northward along JT and KKT (Fig. 1). The propagation speed of these anticyclonic eddies is estimated to be about 1–2 cm s^{-1} along KKT. However, the authors did not distinguish between warm-core and cold-core anticyclonic eddies because SSHA data were used for the identification of eddies. Because the meridional propagation of these eddies has a large influence on not only the heat and salinity budgets but also on water mass formation, such as the North Pacific Intermediate Water (e.g., Shimizu et al. 2001), it is important to determine the water properties of these eddies.

In the present study, we analyzed vertical temperature and salinity profile data to clarify the distribution, structure, and water mass characteristics of warm anticyclonic

eddies (WAE) and cold anticyclonic eddies (CAE; these are referred to simply as warm and cold eddies) in the western boundary region of the North Pacific. The remainder of the manuscript is organized as follows: In section 2, we introduce the data and methods related to eddy identification and examination of the profiles. The distribution of warm and cold eddies, as well as the characteristics of their potential temperature and salinity, is shown in section 3. Finally, section 4 describes the formation and evolution of these eddies and discusses their influence on the transport of heat and materials.

2. Data and methods

a. Eddy identification from SSHA maps

Mesoscale eddies were detected from SSHA maps (“Ref” series based on two satellites, as in IY10) for the period from October 1992 to February 2009, from which the 1993–99 mean had been subtracted. The SSHA maps were produced by Segment Sol Multimissions d’Alimétrie, d’Orbitographie et de Localisation Precise/Data Unification and Altimeter Combination System (SSALTO/DUACS) and distributed by Archiving, Validation, and Interpretation of Satellites Oceanographic data (AVISO), with support from the Centre National d’Études Spatiales (CNES). The horizontal grid interval was about $1/3^{\circ}$. In defining the eddy area, we adopted the same procedure as that used in IY10: that is, that area in which the Okubo–Weiss parameter W is less than the critical value of $-2 \times 10^{-12} \text{ s}^{-2}$ for more than four grid cells (Chelton et al. 2007), without low-pass filtering on either SSHA or W maps. Anticyclonic eddies were recognized based on negative relative vorticity rather than positive SSHA, because SSHA data without low-pass filtering contain seasonal heating–cooling signals. Each detected eddy was tracked by searching for the nearest eddy in a subsequent map within a range of 100 km.

Because the above eddy-detection method is based on W values (negative when rotation is dominant over deformation), horizontal elongation or contraction of eddy shape as a consequence of eddy–eddy and/or eddy–meander interactions result in undetectable eddies in the corresponding SSHA map. In other words, in the present study, some eddies are recognized as being “reborn” after significant eddy–eddy and/or eddy–meander interactions, with the eddy before and after interaction being identified as two distinct eddies. Thus, although the “age” of eddies is shown in section 3, it does not necessarily represent the duration since the time of eddy formation (e.g., shedding from the Kuroshio Extension); in some cases, it is the duration since “rebirth.” Whereas IY10 analyzed eddies with lifetimes $T \geq 4$ weeks, here we selected those with $T \geq 12$ weeks to focus on persistent eddies.

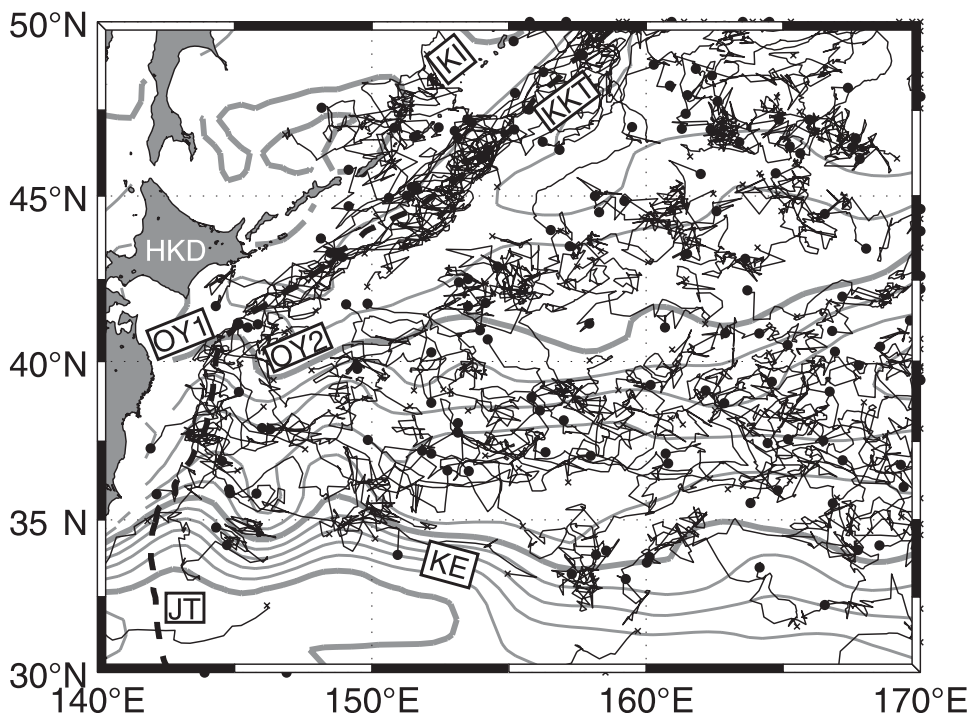


FIG. 1. Trajectories of anticyclonic eddies that lived for longer than 52 weeks, as estimated from SSHA maps. Gray contours and the thick black dashed line are the mean dynamic height (Rio and Hernandez 2004) and the deepest part of the JT and KKT, respectively.

Properties related to the spatial scale and intensity of eddies were calculated for comparison with vertical profiles. Because eddy shape is often distorted by other hydrographic and geographic features, some properties were estimated based on an equivalent Gaussian eddy. The SSHA η of a Gaussian eddy is given by

$$\eta = \eta_0 \exp[-r^2/(2r_0^2)], \quad (1)$$

where η_0 , r_0 , and r are the elevation amplitude, radius, and distance from the eddy center, respectively.

The eddy center was determined from the gravitational center of relative vorticity. The equivalent radius R was calculated based on eddy area A on SSHA maps, as follows:

$$R = (A/\pi)^{1/2}. \quad (2)$$

For axisymmetric eddies, this equivalent radius corresponds to the radius for which the magnitude of geostrophic velocity is maximized: that is, $R = r_0$ for Gaussian eddies. The elevation amplitude of an eddy, calculated for comparison with dynamic height, was also estimated considering an equivalent Gaussian eddy as follows:

$$\eta_0 = \frac{\int_{\text{eddy area}} (\text{SSHA}) dA}{\int_{r \leq R} \exp[-r^2/(2R^2)] dA}. \quad (3)$$

Propagation speed was obtained by calculating the 5-week mean of instantaneous propagation speeds at 1-week intervals. In this paper, the meridional component of the propagation speed c_y is presented.

b. Retrieval of vertical profiles corresponding to the detected eddies

Profiles of potential temperature θ and salinity S , compiled to match the anticyclonic eddies detected from satellite data, were obtained from Argo (Argo Science Team 2001); the World Ocean Database 2005 (WOD05; Boyer et al. 2006); and warm-core rings located east of Japan, as observed in 1997 and 1998 by the Ocean Research Institute, The University of Tokyo (cruises KH-97-3 and KH-98-4 by the R/V *Hakuho-Maru*).

The target area of the present study is 35°–50°N, 140°–155°E, where anticyclonic eddies are densely distributed (IY10). For detailed analyses, we focus on subareas along JT and KKT, which are introduced in section 3a after presenting data on the distribution of heat and salinity

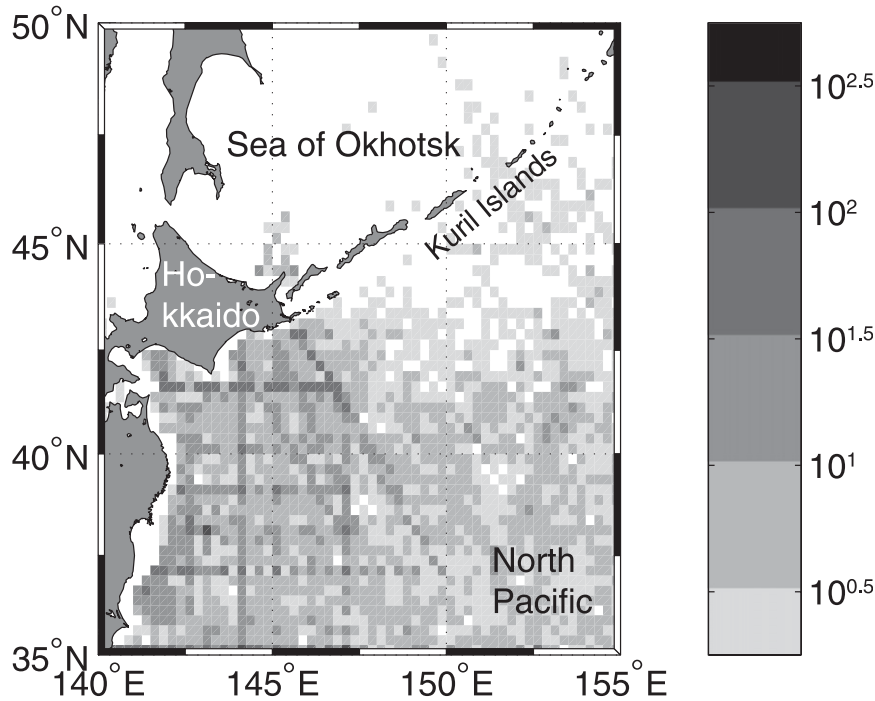


FIG. 2. Data density (number of profiles in each grid cell) for vertical temperature and salinity profiles.

contents. The data density (number of profiles in each grid cell) of vertical profiles is shown in Fig. 2.

The profiles derived from Argo and hydrographic observations generally have vertical resolutions of about 5–50 and 1 dbar, respectively. Intervals with vertical resolutions exceeding 50 dbar were discarded. The remaining data were then interpolated to reference pressure at 5-dbar intervals from the surface to the deepest pressure available using piecewise cubic Hermite interpolation (Fritsch and Carlson 1980). After interpolation, spike-like outliers were excluded using a 5-point median filter (equivalent to a 25-m window). Profiles that still contained obviously unrealistic data, as well as those without near-surface data (data were required to be available from at least 50 dbar), were also excluded from analysis.

Next, profiles measured near the centers of the detected eddies within ± 3 days of the corresponding mapping date were searched for, with respect to the equivalent radius R . The threshold distance was determined considering the correspondence between the dynamic height anomaly (DHA) from the mean field relative to 1500 dbar produced by the Collecte, Localisation, Satellites (CLS) Space Oceanography Division (Rio and Hernandez 2004) and SSHA from satellite altimetry observations. A correspondence was found between SSHA and DHA calculated at 50 dbar relative to 1500 dbar for those eddies for which $r < 0.75R$, as seen in their significant linear

relationship (correlation coefficient $C_r = 0.87$, $p < 0.01$; Fig. 3a, open circles). The correspondence was further improved ($C_r = 0.89$) after adjusting DHA to the value of the center of an equivalent Gaussian eddy, as $DHA_{\text{adjusted}} = DHA/\exp[-r^2/(2R^2)]$ (Fig. 3a, solid circles). However, there were insufficient profiles (110) measured at depths greater than 1500 dbar.

To obtain a general description of eddy structure, we also examined the relationship between SSHA and DHA_{adjusted} for 50–800 dbar. This reference level was considered appropriate because many hydrographic observations are conducted down to 1000 dbar or a slightly shallower depth and 800 dbar is generally deeper than the core depths of anticyclonic warm-core rings previously observed in this area (e.g., Y92). A significant linear relationship between SSHA and DHA_{adjusted} for 50–800 dbar was again found ($C_r = 0.89$). After discarding data that lay outside the 95% confidence interval of the linear regression, we obtained 400 profiles constructed down to depths greater than 800 dbar (Fig. 3).

For some long-lived eddies, multiple profiles were intensively obtained by an Argo float at a frequency of 5–10 days. In such cases, the profile obtained on the day closest to the 15th of the month was selected from those profiles within the same month, to avoid anomalous weighting of a single eddy in constructing a general description of eddy structure in the study area. According to this selection

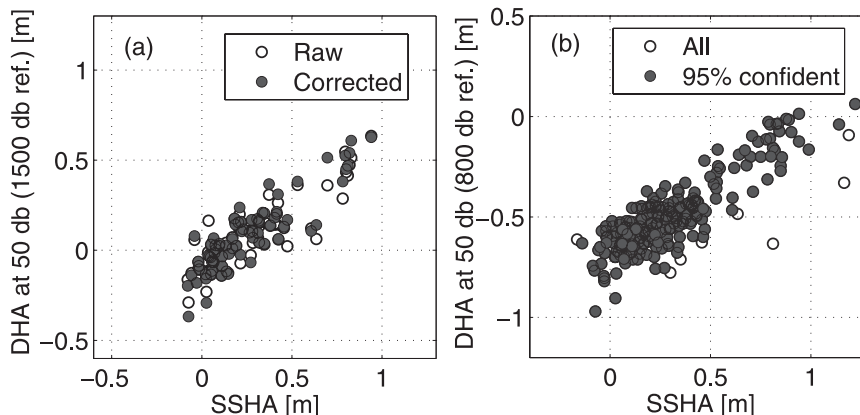


FIG. 3. Relationship between DHA at 50 dbar, as estimated from vertical profiles, and SSHA obtained from satellite altimetry; reference levels for the dynamic height anomalies were (a) 1500 and (b) 800 dbar. In (a), raw and corrected DHA anomalies are plotted against SSHA. In (b), all data are plotted against SSHA. Solid circles indicate data within the confidence interval of linear regression (95% level).

procedure, we finally obtained 227 profiles in the study region, which were identified as 126 individual eddies.

c. Examination of anomalous structure

Because warm-core and cold-core rings were generally identified based on their anomalous water properties relative to ambient water on same depths, we compared the temperature and salinity profiles obtained near the centers of eddies with monthly climatology from *World Ocean Atlas 2001* (WOA01; Conkright et al. 2002), which is expected to represent the basic state (the data after smoothing with horizontal scales far larger than mesoscale eddies are considered to well represent the properties of the ambient waters). Although there could be another option of using datasets constructed by isopycnal averaging, such as Hydrobase (Curry 2001), we select WOA01 that is based on isobaric averaging for our analyses, because data obtained through isopycnal averaging contain information from various depths, which is not consistent with the above identification method of the warm- and cold-core rings. However, as the isopycnal averaging has an advantage for the analyses on isopycnal surfaces, differences between the results using WOA01 and those using Hydrobase (monthly average data with horizontal resolution of 1° with smoothing) were discussed in section 4.

Using monthly $1^\circ \times 1^\circ$ data, vertical profiles of ambient temperature/salinity (T/S) at the locations and for the months of profile measurements were extracted with temporal and spatial interpolation. The WOA01 vertical T/S data were vertically interpolated to pressure levels at every 5 dbar to yield climatological potential temperature and salinity profiles of θ_0 and S_0 . Although the unit of

decibars is used in presenting the results, the term “depth” is used for the vertical coordinate instead of “pressure.”

The characteristics of eddy θ - S profiles were evaluated via mean values with respect to the reference depth and potential density σ_θ . Although mean values with respect to depth are given as the simple arithmetic mean of values at the same depth, mean values with respect to σ_θ were calculated by weighting layer thicknesses on each profile value to consider the contribution of water masses with a thick isopycnal layer.

To identify warm and cold eddies, heat content anomalies (HCA) and salinity content anomalies (SCA) were calculated by the vertical integration of $\theta' = \theta - \theta_0$ and $S' = S - S_0$, as follows:

$$\text{HCA} = \rho_0 C_p \int \theta' dz \quad \text{and} \quad (4)$$

$$\text{SCA} = \int S' dz, \quad (5)$$

where ρ_0 and C_p are the reference density and the heat capacity of seawater, respectively. As performed in estimating the dynamic height anomaly, heat and salinity contents from raw profile values were adjusted to those at the center of the eddy: for example, using $\text{HCA}_{\text{adjusted}} = \text{HCA}/\exp[-r^2/(2R^2)]$. The Eulerian mean meridional transports of heat and salinity for an area A_0 were estimated by multiplying the frequency of eddy occurrence from the satellite altimetry data by the ensemble mean of the transport from the hydrographic data, as follows:

$$\overline{v'\theta'} = \frac{N_{\text{satel}}}{T_{\text{obs}} A_0} \left(c_y \int_0^R \theta' r dr \right)_{\text{eddy}} \quad \text{and} \quad (6)$$

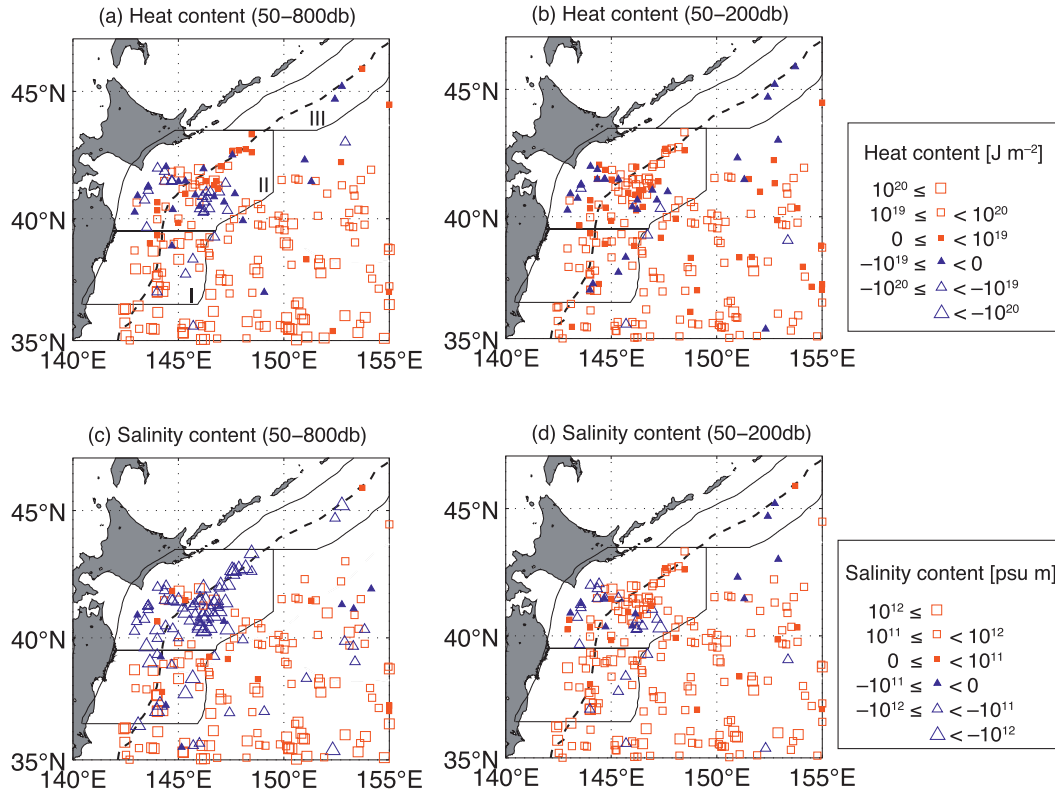


FIG. 4. Heat and salinity contents: (a) heat content integrated over 50–800 dbar, (b) heat content integrated over 50–200 dbar, (c) salinity content integrated over 50–800 dbar, and (d) salinity content integrated over 50–200 dbar.

$$\overline{v'S'} = \frac{N_{\text{satel}}}{T_{\text{obs}}A_0} \left(\overline{c_y \int_0^R S'r dr} \right)_{\text{eddy}}, \quad (7)$$

where the area integration was conducted within an equivalent Gaussian eddy; the overbars on the rhs of the equations indicate the ensemble mean of eddy profiles measured in the area; and N_{satel} and T_{obs} denote the number of eddies identified in SSHA maps from satellite altimetry data and the duration of the satellite observation period (830 weeks), respectively.

Although anomalies in heat and salinity content were used to classify the type of core water, a profile of layer thickness specifies a core layer that compensates surface elevation. Following previous studies (e.g., Talley 1988), we defined the planetary contribution of potential vorticity as follows:

$$Q = -\frac{f \partial \sigma_\theta}{\rho \partial z}. \quad (8)$$

3. Results

a. Distribution of anticyclonic eddies with warm or cold cores

To clarify the distribution of eddies with various core-water properties in the upper layer, we calculated

anomalies in heat and salinity content by integrating over the depth ranges of 50–800 and 50–200 dbar (Fig. 4). Eddies with positive and negative heat (salinity) anomalies are referred to as warm and cold (fresh and saline) eddies, respectively. For both reference depth ranges (50–800 and 50–200 dbar), warm eddies were predominant over a wide area, with higher heat contents at lower latitudes (Figs. 4a,b). Cold eddies occurred mainly in areas located inshore and offshore of the trench line (but not on the line itself) southwest of Hokkaido (HKD), although some were also found farther north at about 46°N, off the Kuril Islands (KI). The former distribution roughly corresponds to the mean location of the two southward intrusions of the Oyashio (OY1 and OY2 in Fig. 1; Kawai 1972). As seen in the distribution, fewer cold eddies were identified in the relatively shallow range of 50–200 dbar (49 and 33 cold eddies by the integrations over 50–800 and 50–200 dbar, respectively). By taking a range of 50–400 dbar instead of 50–200 dbar, we observed a slight increase in the number of cold eddies to 42, whereas a range of 50–100 dbar yielded 34 cold eddies. This finding indicates that some eddies in the Oyashio area southwest of Hokkaido have positive and negative θ anomalies, typically above and below 200 dbar, respectively.

Although the obtained distribution of saline–fresh eddies is similar to that of warm–cold eddies, the saline–fresh ratio is smaller than the warm–cold ratio, especially above 800 dbar: saline–fresh ratios were $138/89 = 1.55$ (50–800 dbar) and $191/36 = 5.31$ (50–200 dbar), and warm–cold ratios were $178/49 = 3.63$ (50–800 dbar) and $194/33 = 5.88$ (50–200 dbar). The distribution of warm eddies is different from that of saline eddies along the trench line southwest of Hokkaido, where eddies have positive heat and negative salinity anomalies at depths of 50–800 dbar.

The above complexities evident in the vertical profiles are primarily attributable to the occurrence of a strong halocline in the upper layer of the subarctic region, where the subsurface temperature minimum is attained (Ueno and Yasuda 2000). If a warm and saline water mass in the upper layer of the Kuroshio Extension is shed to the subarctic region and depresses the cold and fresh surface layer downward, then the upper layer becomes warm and saline compared with the ambient waters of the same depth, whereas the depressed layer is cold and fresh. Because the surface water is depressed along with the isopycnal surface, it is not colder or fresher than the water on the same isopycnal surface; this differs from the case of anticyclonic eddies with cold and fresh cores generated by the direct input of cold and freshwater (on isopycnal surfaces) from the Sea of Okhotsk (Y00).

To discriminate between anticyclonic eddies with and without warm cores, we simply consider the sign of the heat content anomaly for the depth range of 50–200 dbar. Discrimination based on the properties on isopycnal surfaces is difficult because the core waters of anticyclonic eddies in this region generally outcrop at the surface.

Below, we focus on eddies within 2° latitude of the trench lines where a dense contribution of intense anticyclonic eddies was reported previously (IY10) and profiles of both warm and cold eddies are obtained. Based on the horizontal distribution of the heat content anomaly integrated over the depth range of 50–200 dbar (Fig. 4b), we classified eddies into four groups: group I, warm eddies in subarea I (between 36°N and $39^\circ30'\text{N}$); group IIw, warm eddies in subarea II (north of $39^\circ30'\text{N}$ and west of $149^\circ30'\text{E}$); group IIc, cold eddies in subarea II; and group III, cold eddies in subarea III (east of $149^\circ30'\text{E}$ and south of 43°N).

b. Eddy properties

Figure 5 shows the frequency distributions of the ages (weeks since initial identification in an SSHA map), elevation amplitudes, equivalent radii, and meridional propagation speeds of the four groups of eddies. Because the profiles of one extremely long-lived eddy (LLE; tracked from September 2001 to June 2005),

mainly observed by Argo floats, the contribution of LLE profiles is highlighted.

LLE was mainly observed as a warm eddy (group IIw, 17 profiles), although sometimes as a cold eddy (group IIc, 4 profiles). Changes in classification occurred in summer–fall 2003 (from a warm eddy to a cold eddy) and in late 2003 (from a cold eddy to a warm eddy). Although the former change was caused mainly by the evolution of the vertical temperature profile, the latter was also related to northeastward propagation of the eddy, which caused a change in the climatological profiles used as a reference and resulted in an enhanced temperature anomaly. The detailed evolution of this particular eddy is not considered here, because it is beyond the scope of this study.

Eddies of group I were generally young and strong: their ages were less than 36 weeks and the mode of the amplitude was 0.3–0.4 m, which is the strongest among the four groups. The range in radius was 40–100 km and the mode was found in the 50–60-km bin. The northward propagation speed varied in an apparently random manner from -5 to 5 cm s^{-1} .

Although distributed in the same subarea, warm eddies (group IIw) were generally older, stronger, and larger than cold eddies (group IIc); however, as mentioned above, long-lived eddies were sometimes classified as cold eddies. Three eddies (three profiles) of group IIw, including LLE, were older than 52 weeks, whereas no eddy was older than 52 weeks in group IIc (Fig. 5a). The modes of the amplitude and radius were 0.2–0.3 m and 60–70 km for group IIw and 0–0.1 m and 40–50 km for group IIc, respectively. Northward movement was recognized for group IIw, with typical speeds of up to 2 cm s^{-1} , whereas no northward movement was recorded for group IIc eddies, which actually showed a slight southward tendency with a mode of -2 to -1 cm s^{-1} .

The three cold eddies of group III were younger than 36 weeks, with amplitudes, radii, and propagation speeds in the ranges of 0–0.3 m, 30–50 km, and -1 to 2 cm s^{-1} , respectively.

c. Trajectories

The eddy trajectories are complicated (Fig. 6), possibly because of vigorous interactions with other eddies (as observed by Y92). Because we identified eddies before and after rebirth (as explained in section 2a), initial points were distributed in areas far from the source water region of the Kuroshio Extension or the area off the Kuril Islands. However, the trajectories of eddies in each group still provide valuable information on the origin and fate of eddies.

Several group I eddies originated from an offshore area and the northern area of the Kuroshio Extension, and two eddies migrated to north of 40°N , one of which was also

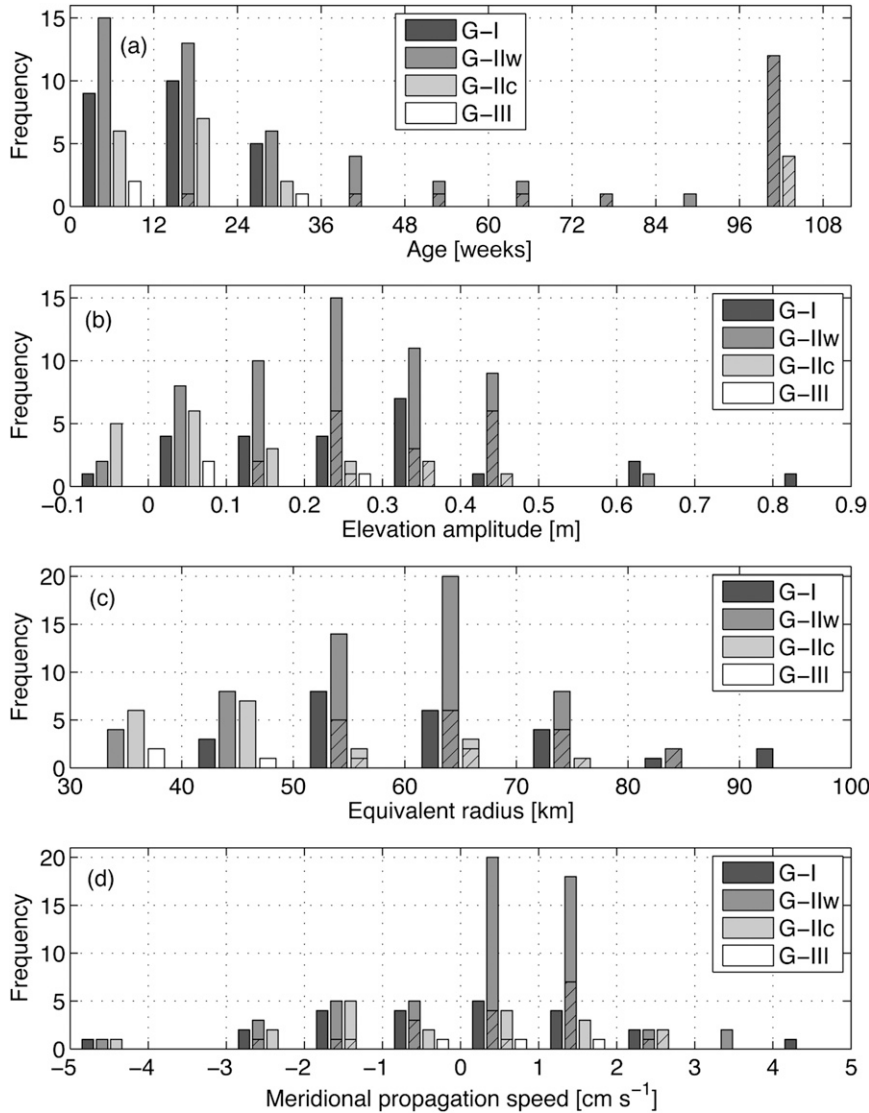


FIG. 5. Frequency distributions of (a) age, (b) elevation amplitude, (c) equivalent radius, and (d) meridional propagation speed for eddy groups I, IIw, IIc, and III. Hatching indicates the contribution of a single LLE; age classes greater than 96 weeks were assigned to a single bin because the last profile observed within LLE was 1172 days after its first detection in a SSHA map, which is a much longer period than that obtained for other eddies, and the range of “older than 96 weeks” was not available for other profiles.

observed in subarea II as a warm eddy; however, no long-distance propagation was recognized (Fig. 6a). Remarkable long-distance propagations to the area near Hokkaido and the Kuril Island were seen for groups IIw (Fig. 6b) and IIc (Fig. 6c). The eddy that reached the Etorof Strait between the islands of Etorof (ET) and Urup (UR) was LLE (as mentioned above, which was categorized into both groups IIw and IIc). In subarea II, warm eddies (group IIw) showed a northeastward trend along KTT (Fig. 6b; see also Fig. 5d), whereas this trend was not observed for cold eddies (group IIc), except for

LLE (Fig. 6c). Similar to group I, some of the group IIw eddies originated from the south and southeast (Fig. 6b). One notable case in group IIc was a southwestward-moving eddy that originated from the north, near Kunashiri Island (KN; Fig. 6c). Among the three eddies of group III, one moved north toward Simushir Island (SM; Fig. 6d).

d. Vertical profiles and meridional transports of heat and salinity

The previous two subsections considered the horizontal distribution of heat–salinity contents and eddy properties

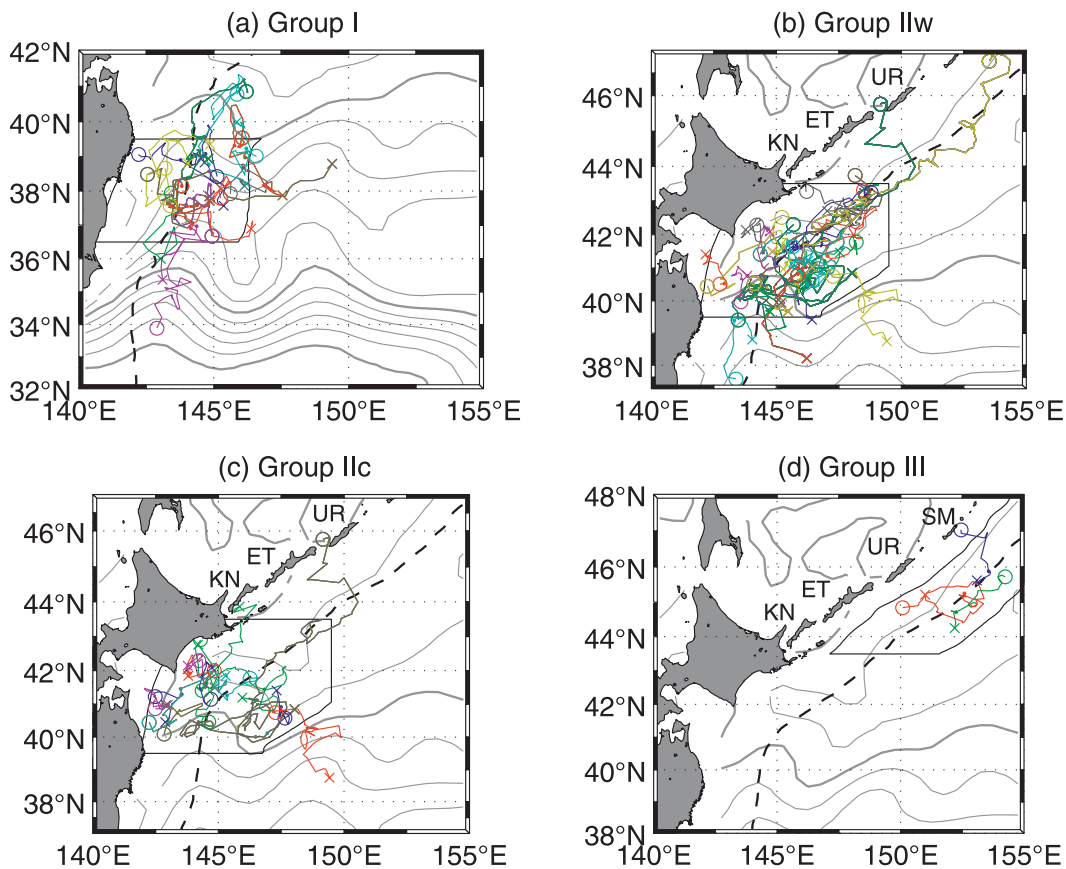


FIG. 6. Trajectories of eddies in groups (a) I, (b) IIw, (c) IIc, and (d) III. Small solid circles, crosses, and open circles indicate the positions of profiles, first detection of the eddy from an SSHA map, and final detection from an SSHA map, respectively.

derived from analyses of altimetry data. Here, we examine vertical profiles of θ and S for eddies from the four sub-areas, their anomalies from the climatology, and associated meridional transports of heat and salinity.

1) VERTICAL PROFILES OF GROUP I EDDIES

Group I eddies typically had warm, saline, and less dense core water above 300 dbar, with relatively weak vertical gradients (Figs. 7a–c). At 200 dbar, values of θ and S were $12.4^\circ \pm 3.4^\circ\text{C}$ (mean \pm standard error) and 34.4 ± 0.28 psu, respectively, being warmer and saltier than the mean climatological values of 8.1°C and 34.0 psu, although θ was slightly colder than the indicative temperature of the Kuroshio Extension (14°C at 200 m; Kawai 1969). Based on the mean profiles, the minimum σ_θ anomaly was $-0.51\sigma_\theta$ at 245 dbar, with a positive θ anomaly of 4.31°C and an S anomaly of 0.30 psu. The θ anomaly was positive, whereas the S anomaly became significantly negative below 425 dbar.

Profiles of θ , S , and pressure on isopycnal surfaces in the range from $26.00\sigma_\theta$ to $27.00\sigma_\theta$ are shown in Figs. 7d–f.

Although this range in σ_θ corresponds to the lower part of the core, the depth of the mean eddy profile was significantly deeper (by about 150 dbar) than the ambient profile, at least up to $27.00\sigma_\theta$ (Fig. 7f). Also of note, the temperature and salinity values are much lower than those of the climatological mean at around $26.70\sigma_\theta$ (Figs. 7d,e), although the mean temperature of eddy profiles is warmer than the climatology at a given depth (Fig. 7a). The largest difference between profiles and the climatology was observed at $26.65\sigma_\theta$, where the difference from the climatology was -1.3°C for temperature and -0.19 psu for salinity.

2) VERTICAL PROFILES OF GROUP IIW EDDIES

Warm, saline, and less dense cores in the upper layers above 300 dbar were also recognized for warm eddies in subarea II (group IIw; Figs. 8a–c). For these eddies, the magnitudes of θ and S were less than those of group I eddies, and positive anomalies were confined to the shallower layer: a positive θ anomaly was not significant below 350 dbar and the S anomaly became negative

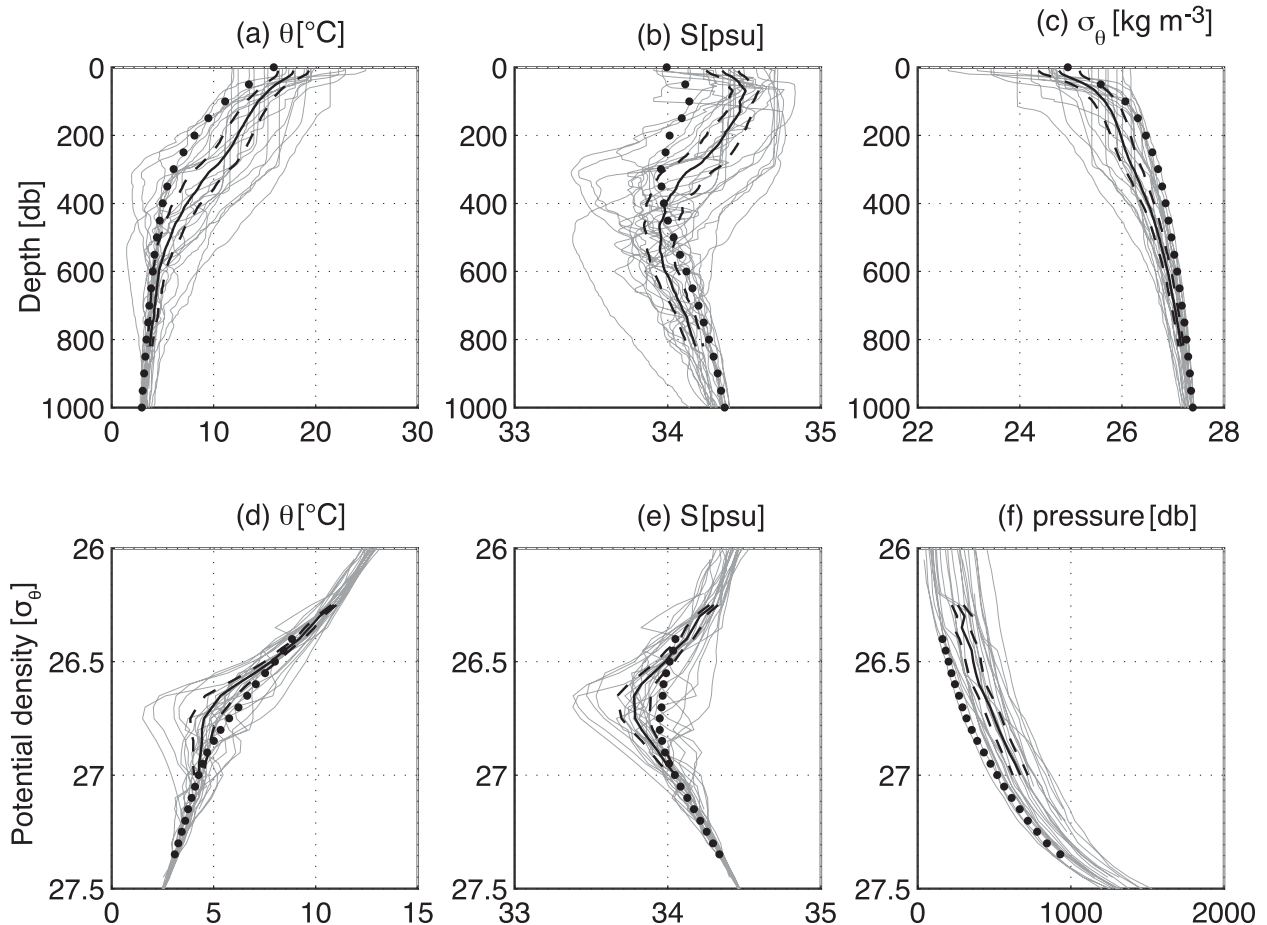


FIG. 7. Vertical profiles of group I eddies, showing (a) potential temperature ($^{\circ}\text{C}$), (b) salinity (psu), and (c) potential density with respect to depth (kg m^{-3}), and (d) potential temperature ($^{\circ}\text{C}$), (e) salinity (psu), and (f) depth with respect to potential density (dbar). Solid (dashed) lines are the mean plus (minus) standard error of eddy profiles, and black dotted lines indicate the mean of climatological profiles (as obtained at the locations of eddy profiles).

below 250 dbar. At 100 dbar, θ and S were $8.1^{\circ} \pm 3.0^{\circ}\text{C}$ (mean \pm standard error) and 33.9 ± 0.29 psu, respectively, colder and fresher than group I eddies but warmer and saltier than ambient values of 5.2°C and 33.6 psu. Negative σ_{θ} anomalies penetrated to a deeper layer than was the case for group I eddies. The minimum σ_{θ} anomaly was $-0.20\sigma_{\theta}$ at 370 dbar. As mentioned above, mean profiles of θ and S did not show a significant positive anomaly at this depth: mean anomalies of θ and S from the climatology were 0.04°C (less than the standard error of 0.48°C) and -0.22 psu, respectively, indicating that group IIw eddies were no longer “pure” warm eddies but contained a significant component of freshwater.

On isopycnal surfaces, we again found a depression of isopycnal surfaces and relatively low θ - S values at around $26.70\sigma_{\theta}$ (Figs. 8d-f), as for group I eddies, although mean values of all profiles could not be defined above $26.70\sigma_{\theta}$. In calculating the mean values at $26.70\sigma_{\theta}$

using the available profiles, we obtained mean differences between the eddy and climatological profiles of -1.29°C in θ and -0.15 psu in S . Although these values are similar to those for group I, the profile values of $2.6^{\circ} \pm 0.26^{\circ}\text{C}$ (mean \pm standard error) and 33.5 ± 0.03 psu are significantly colder and fresher than the modal values of group I (5.2°C and 33.8 psu). The modal values are used instead of the means, because the mean temperature and salinity of group I eddies yielded a denser value than $26.70\sigma_{\theta}$ because of their relatively wide range and nonlinear contributions to potential density.

3) VERTICAL PROFILES OF GROUP IIc EDDIES

Profiles of cold eddies in subarea II (group IIc; Figs. 9a-c) are completely different from those of group IIw eddies in that they generally have cold and fresh anomalies for the upper layer above 800 dbar. Negative temperature and salinity anomalies are pronounced

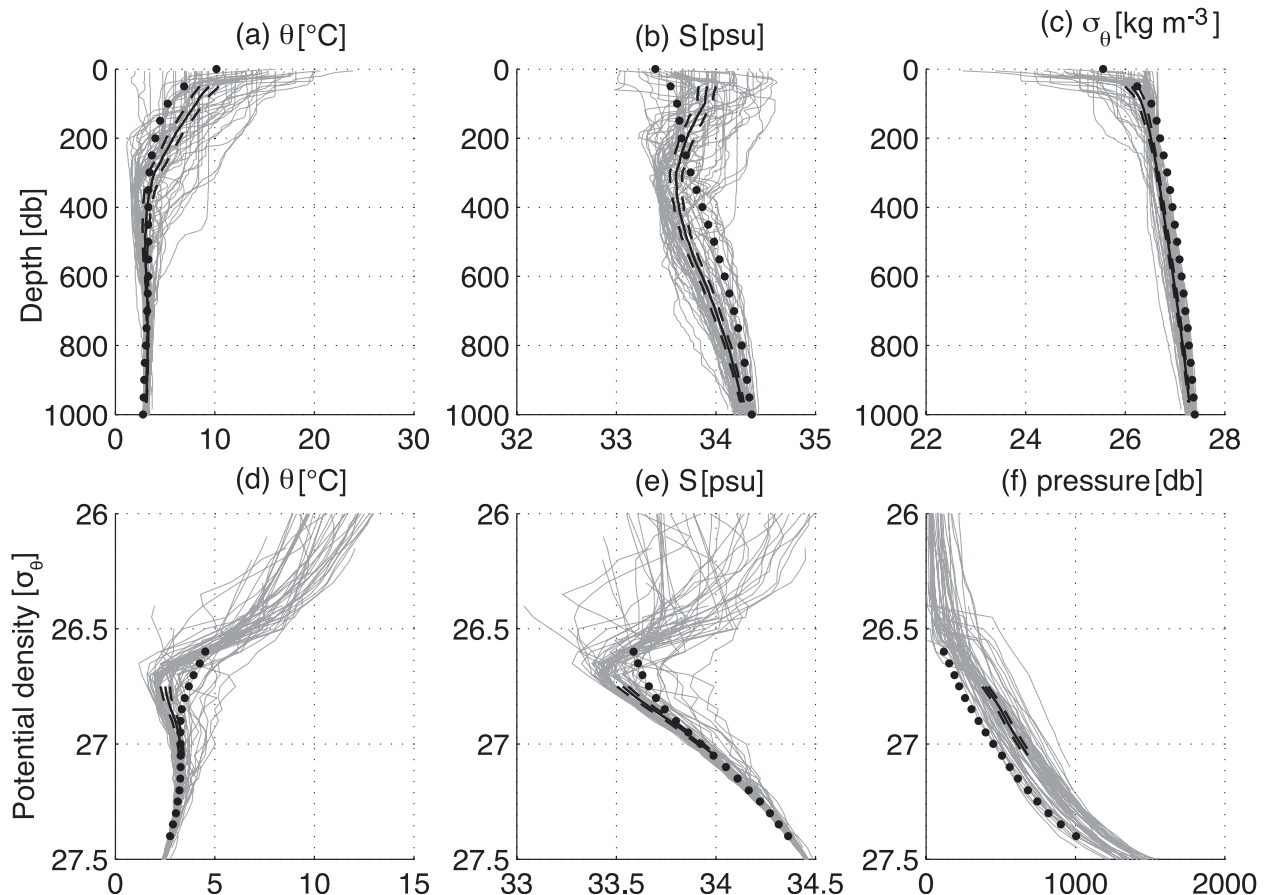


FIG. 8. As in Fig. 7, but for group IIw eddies.

near the surface and are increased (approaching zero) with increasing depth. The values of θ and S at 100 dbar were $3.7^\circ \pm 2.7^\circ\text{C}$ (mean \pm standard error) and 33.4 ± 0.33 , respectively, being colder and fresher than the climatological values of 5.6°C and 33.6 psu. The mean θ value of 3.7°C is colder than the indicative temperature of the Subarctic Front (4°C at 100 m).

The profiles on isopycnal surfaces in the range $26.50\sigma_\theta$ – $27.00\sigma_\theta$ (Figs. 9d–f) are similar to those of group IIw in that they have lower temperature and salinity values than the climatology at around $26.70\sigma_\theta$. Although the ensemble mean of all profiles could not be calculated above $27.00\sigma_\theta$, the mean values (\pm standard error) at $26.70\sigma_\theta$, as calculated from the available profiles, were $2.0^\circ \pm 0.34^\circ\text{C}$ in temperature and 33.4 ± 0.03 in salinity; the differences from climatological values were -1.97°C and -0.22 psu, respectively.

4) VERTICAL PROFILES OF GROUP III EDDIES

In subarea III, water temperature was colder than 4°C below 40 dbar and background stratification was maintained mainly by the salinity gradient (Figs. 10a–c).

Although one of the three eddy profiles was very close to the climatological mean, the other two had cold, fresh, and less dense anomalies in the layer below 100 dbar. The former profile had a significant temperature anomaly only near the surface; hence, it did not have negative heat content when integrated down to 800 dbar. The θ and S profiles on isopycnal surfaces were again significantly lower than the climatology in the range around $26.60\sigma_\theta$ – $26.70\sigma_\theta$, and the difference between the means of the eddy and climatological profiles was largest at $26.60\sigma_\theta$ (Figs. 10d–f). At $26.60\sigma_\theta$, the mean θ and S values were 1.7°C and 33.4 psu, respectively, with the difference from the climatology being -0.48°C and -0.04 psu.

5) PROFILES OF POTENTIAL VORTICITY

Figure 11 shows profiles of Q [Eq. (4)] on isopycnal surfaces from $26.40\sigma_\theta$ to $27.20\sigma_\theta$. Although the profiles are noisier than the θ and S profiles because of vertical differentiation, the mean of available eddy profiles is significantly lower than the climatology in the range of $26.60\sigma_\theta$ – $26.80\sigma_\theta$ for group IIw (Fig. 11b) and in the

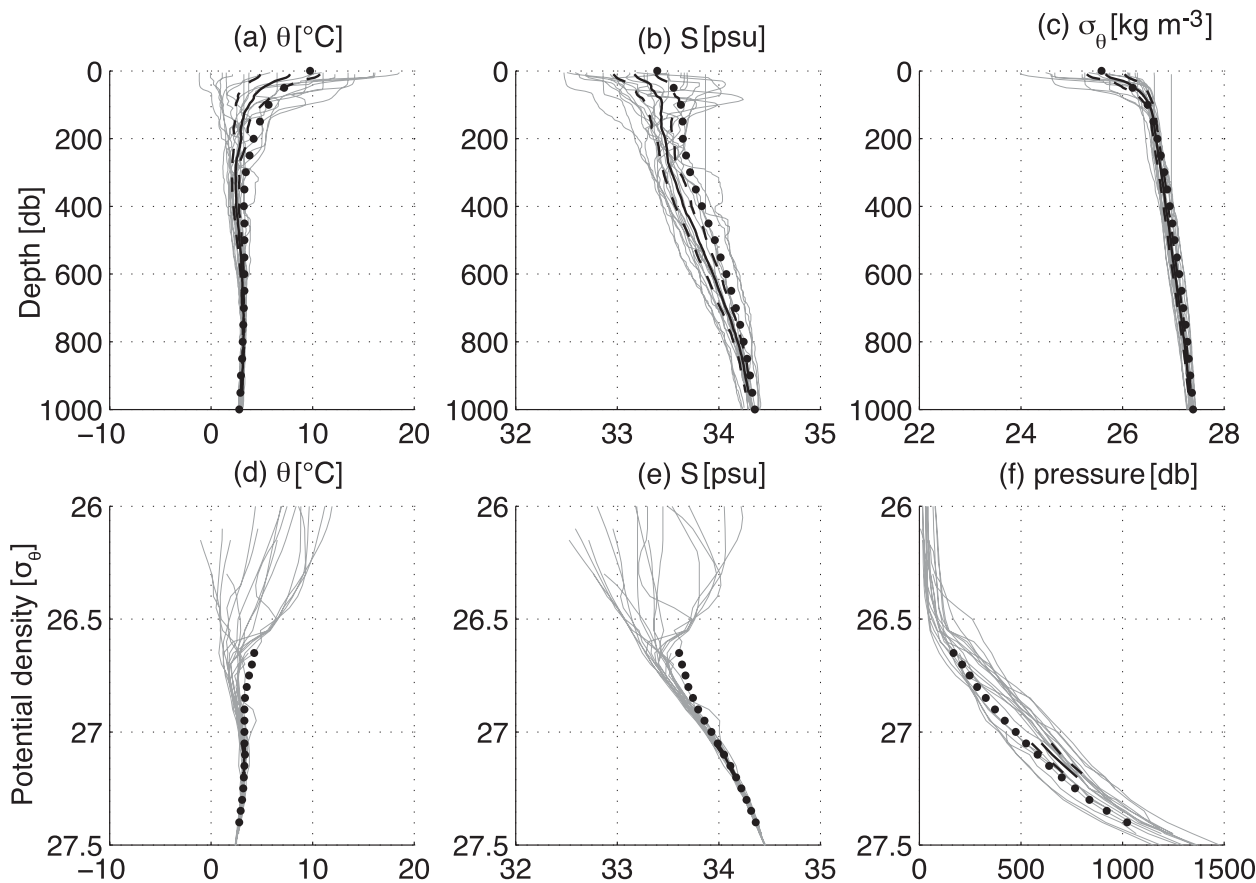


FIG. 9. As in Fig. 7, but for group IIc eddies.

range of $26.75\sigma_\theta$ – $26.80\sigma_\theta$ for group IIc (Fig. 11c). Two of the three profiles of group III also had lower Q values than the climatology in the range of $26.65\sigma_\theta$ – $26.86\sigma_\theta$ (Fig. 11d). Group I eddies only showed significant negative Q anomalies above $26.40\sigma_\theta$. The Q values of the eddy profiles were not clearly lower than the climatology in this range, but they were lower above $26.40\sigma_\theta$ (Fig. 11a).

Given that the above potential density range of $26.60\sigma_\theta$ – $26.80\sigma_\theta$ corresponds to a layer of θ and S minima on isopycnal surfaces, we examined the relationship between S and Q at $26.70\sigma_\theta$ (Fig. 12). A significant positive relationship was found between S and Q for groups I ($r = 0.49$, $p = 0.02$), IIw ($r = 0.38$, $p = 0.00$), and IIc ($r = 0.51$, $p = 0.03$). Although group I was generally more saline, the relationship showed roughly the same trend. Two of the group III eddies (the third eddy had extremely weak anomalies) also plotted along this trend, in the lowest salinity range.

6) HEAT AND SALINITY TRANSPORTS

Because the eddy profiles show θ and S anomalies, the meridional movement of eddies caused heat and salinity

transports. According to Eqs. (6) and (7), we obtained significant heat and salinity transports in subarea II (caused by group IIw and IIc eddies; Fig. 13). The group IIw eddies made the greatest contribution because of their significant northward propagation (not shown in the figure; see also Fig. 5). A significant mean positive heat transport was found in the upper layer above 400 dbar, whereas large mean positive and negative salinity transports were recognized in layers above and below 250 dbar, respectively. Vertical integration from the surface to 200 dbar (the approximate maximum depth of the mixed layer in this area) and zonal integration across subarea II (the zonal extent of 4° latitude) yielded an upper-layer heat transport of 0.8 TW and salinity transport of $23 \times 10^3 \text{ psu s}^{-1}$. The mean salinity transport in the lower layer (250–800 dbar) was $-48 \times 10^3 \text{ psu s}^{-1}$.

e. Typical eddy structures

Although several hundred profiles were observed near the centers of eddies in the study area, many are spatially isolated profiles obtained from Argo. However, some transect data crossing eddies are available, with a

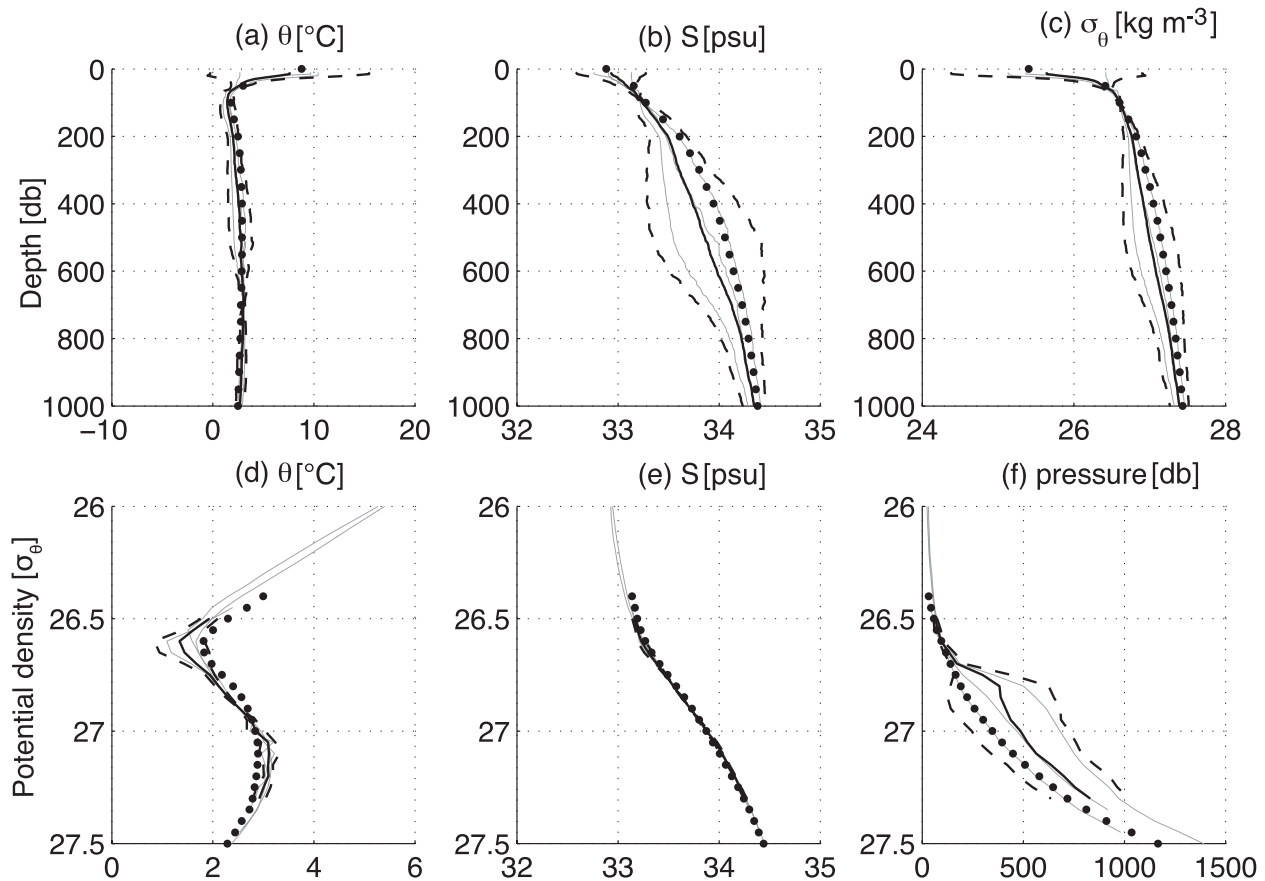


FIG. 10. As in Fig. 7, but for group III eddies.

vertical extent of 2000 m, mainly obtained by the Japan Meteorological Agency (JMA). We compiled representative cross sections of eddies from groups I (eddy I-02; Fig. 14a), IIw (eddy IIw-04; Fig. 14b), and IIc (eddy IIc-01; Fig. 14c), using data observed by JMA in February 2002, May 2004, and April 2001, respectively. Cross sections of θ and S for these eddies are shown in Fig. 14, together with maps showing their trajectories, radii, and transects.

Eddy I-02, recognized in SSHA maps from November 2001, had a clear warm and saline core with a temperature of 15° – 16°C , salinity of 34.7–34.8 psu, and thickness of about 300 m (Fig. 14a). Here, θ and S were similar to those of the surface water of the Subtropical Mode Water in winter (16° – 18°C and 34.7–34.8 psu, respectively; Suga et al. 1989), indicating the direct influence of the Kuroshio Extension. Isolines of θ and S below the core are seen to strongly outcrop on both sides of the core, especially on the northern side. Although the 4°C isotherm is seen at 900 dbar at the center, it appears at the surface at 1° north of the center. The depression of temperature and salinity isolines was recognized down to at least 2000 dbar. In addition, fresh and cold water masses

with relatively small horizontal and vertical scales were distributed below the core, close to the $26.7\sigma_{\theta}$ isopycnal.

Eddy IIw-04 was identical to LLE, which was recognized in SSHA maps from September 2001 (Fig. 14b). Core water in the upper 200 dbar was warmer and saltier than ambient water, although much colder (4° – 8°C) and fresher (33.6–33.8 psu) than I-02. There existed a markedly cold ($<2^{\circ}\text{C}$) and fresh (<33.5 psu) water mass below the core, with patchy structure along $26.70\sigma_{\theta}$, as in I-02. Vertical penetration was evident down to 2000 dbar, whereas a slight offshore shift of the eddy axis (position of maximum amplitude) is recognized in a layer below 1500 dbar.

Unlike the above warm eddies, the core of eddy IIc-01 in the upper 300 dbar consisted of cold and freshwater (Fig. 14c). The eddy trajectory suggests that the core water originated from the Sea of Okhotsk. The core water of IIc-01 was different from the cold and freshwater masses below the core of the warm eddies in that the former was slightly colder (0° – 2°C), fresher (<33.4 psu), and less dense ($26.60\sigma_{\theta}$ at the middle of the core) than the latter. Although this eddy had a narrow horizontal extent, the depression of the salinity anomaly extends to 1500 dbar,

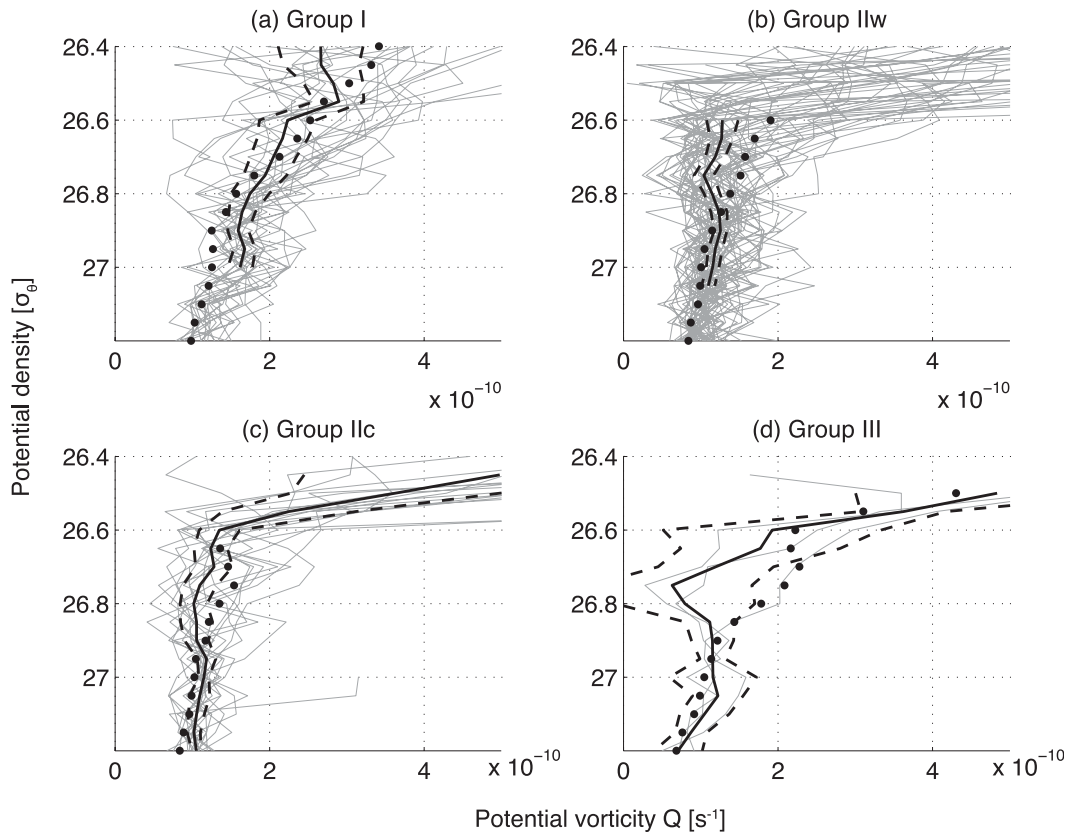


FIG. 11. Potential vorticity Q vs potential density for eddies from groups (a) I, (b) IIw, (c) IIc, and (d) III. Solid (dashed) lines are the mean plus (minus) standard error of eddy profiles, and black dotted lines indicate the mean of climatological profiles.

and we observed an offshore shift in the eddy axis, as also seen in IIw-04.

4. Discussion

Although the analyses of the anomalous structure of the eddies in the present study were based only on the *WOA01* climatology constructed through isobaric averaging, similar results can be obtained using Hydrobase based on isopycnal averaging. However, we note here several differences caused by the difference in climatology, for future studies. The differences are mainly caused by the difference in sharpness of subsurface salinity minimum obtained from the two climatologies. Because the salinity minima were observed in the specific potential density range of $26.6\sigma_\theta$ – $26.8\sigma_\theta$ (Yasuda et al. 1996), the isopycnal averaging reproduces sharper minimum than the isobaric averaging, with respect not only to potential density but also to depth. However, because the depths of $26.6\sigma_\theta$ – $26.8\sigma_\theta$ are variable profile by profile, employing the sharp minimum at a fixed depth as a mean state causes overestimation

(underestimation) of positive (negative) salinity anomalies in this depth range, which was up to about 0.1 psu in our analyses. Similarly, errors in the temperature anomaly with respect to fixed depths were found to be up to 0.8°C . On the contrary, the isopycnal averaging has an advantage for the analyses on isopycnal surfaces. Because temperature and salinity minima at $26.6\sigma_\theta$ – $26.8\sigma_\theta$ are smoothed by the isobaric averaging, the negative anomalies estimated with *WOA01* might be overestimated by up to $\sim 0.7^\circ\text{C}$ and ~ 0.1 psu, respectively. It is noted, however, these differences do not change signs of the anomalies that were found in the range of the salinity minimum and hence do not affect the general results.

In the present study, an analysis of SSHA maps and vertical profiles of temperature and salinity confirmed the occurrence of warm and cold anticyclonic eddies and revealed their characteristics, in and around the Oyashio, typically along JT and KKT. Based on these results, Fig. 15 shows a schematic model of the formation and evolution of the warm and cold eddies. The main features of the basic field are the warm and saline Kuroshio

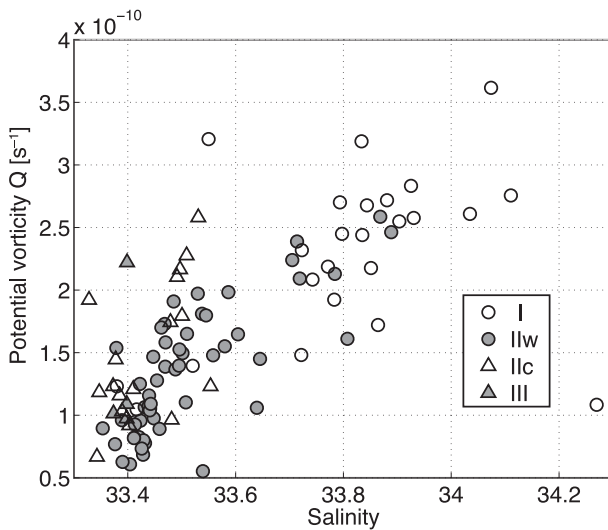


FIG. 12. Relationship between salinity (psu) and potential vorticity Q at the $26.70\sigma_{\theta}$ isopycnal surface.

Extension in the south and the cold and fresh Oyashio in the north (Fig. 15a). Because the Oyashio has two major sources, consisting of 1) extremely cold, fresh, and low-potential-vorticity Sea of Okhotsk water (OSW) and 2) relatively warm, saline, and high-potential-vorticity water from the East Kamchatka Current (EKC), we consider

the Oyashio water (OYW) as being moderately cold, fresh, and with low potential vorticity. Part of the moderately cold and freshwater is detached from the Oyashio and intrudes below the jet of the Kuroshio Extension; these two waters then flow eastward together (Kawai 1972; Yasuda et al. 1996). Yasuda et al. (1996) demonstrated that mixing of this Oyashio water with Kuroshio water produces North Pacific Intermediate Water, which is widely distributed throughout the subtropical North Pacific.

Although the Oyashio includes a contribution from EKC, anticyclonic eddies may form by a contribution derived mainly from the Sea of Okhotsk, with extremely cold, fresh, and low-potential-vorticity water in the core (Fig. 15b; categorized into group IIc and III eddies). Although the distribution of such eddies roughly corresponds to the mean location of the Oyashio southward intrusions (OY1 and OY2 in Fig. 1), they are not generated by the shedding of these intrusions with cyclonic flows. The distribution of anticyclonic eddies around OY1 and OY2 can be explained if the eddies are transported along the flow of the Oyashio. The distribution of the cold-core anticyclonic eddies around OY1 is consistent with that reported by Shimizu et al. (2001), but we found that the eddies also occur in offshore areas, mainly around OY2.

Warm anticyclonic eddies are shed from the Kuroshio Extension to the north (Fig. 15b). Although many warm

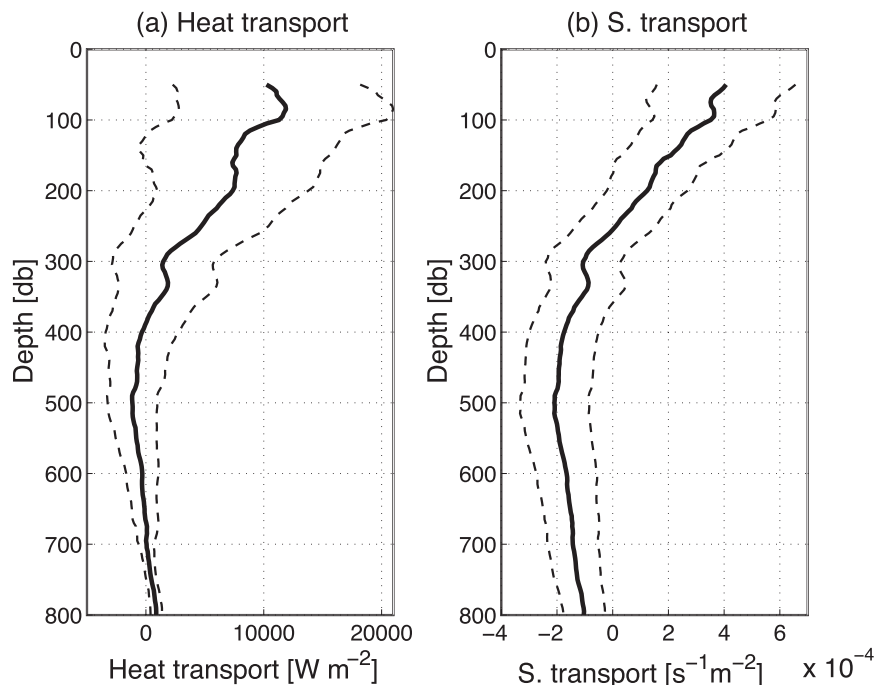


FIG. 13. Mean northward transports of (a) heat and (b) salinity ($\text{psu s}^{-1} \text{m}^{-2}$, solid lines) averaged within subarea IIw. Dashed lines indicate the upper and lower limits of one-sided 95% confidence intervals (therefore, the area between the dashed lines represents the 90% confidence interval).

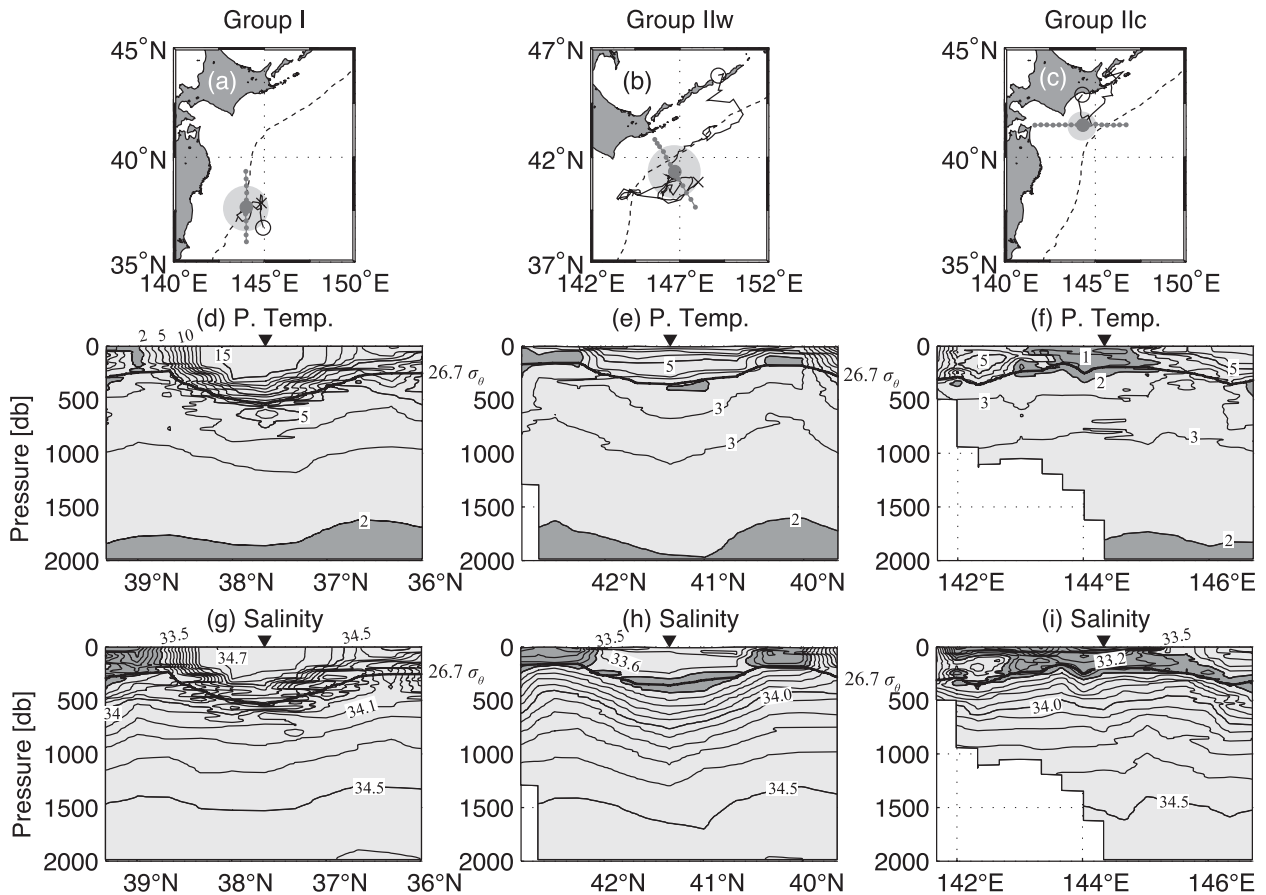


FIG. 14. Structure of representative eddies of (left to right) groups I, IIw, and IIc: (a)–(c) Trajectories and lines of hydrographic observations; vertical cross sections of (d)–(f) potential temperature and (g)–(i) salinity for corresponding eddies. In (a)–(c), trajectories, initial points, final points, area of equivalent Gaussian eddies, and hydrographic transects are shown with solid lines, open circles, crosses, light gray shading, and dark gray lines and points, respectively. In (d)–(i), water masses colder than 2°C and fresher than 33.5 psu are shaded in dark gray, and thick contour lines depict the $26.70\sigma_{\theta}$ isopycnal surface.

eddies have been observed near the east coast of Japan, they also form in eastern areas and propagate westward (IY10). The distribution of warm eddies extends northeastward along KKT. IY10 detected the northeastward translation of anticyclonic eddies along the trench, but the present findings indicate that these eddies have a warm core and originated from the Kuroshio Extension. As a result of vigorous eddy–eddy and/or eddy–meander interactions near the Kuroshio Extension, these newly generated eddies (mainly group I eddies) were not tracked for long distances by the method employed in the present study (Fig. 6). The cold and fresh anomalies below the warm core of these eddies is suggested to be the Oyashio water, which occurs below the Kuroshio Extension jet and is shed to the north along with the upper layer (see the following paragraph for further details).

During the long period that warm eddies detached from the Kuroshio Extension remain in the area north of the extension, their structure shows a gradual change

(Fig. 15c), as recognized by the difference between warm eddies in subareas I (group I eddies) and II (group IIw eddies). First, the warm and saline core water became cooler and fresher over time, and the thickness of the core decreased. However, water columns with a negative σ_{θ} anomaly did not shrink as much as those with positive θ and S anomalies. The minimum of the mean σ_{θ} anomaly of group IIw eddies occurred at a greater depth than that for group I eddies. Thus, group IIw eddies were not simply warm eddies: they had double cores, comprising a warm and saline upper core, and a cold and fresh lower core, both of which were less dense than ambient water at the same depth. This double-core structure has been observed previously (e.g., Y92; Talley et al. 1995), although a general and quantitative description is presented here for the first time. The mean water properties of the lower core were colder and fresher than those of the climatology at the same potential density. We also consider that the structure of

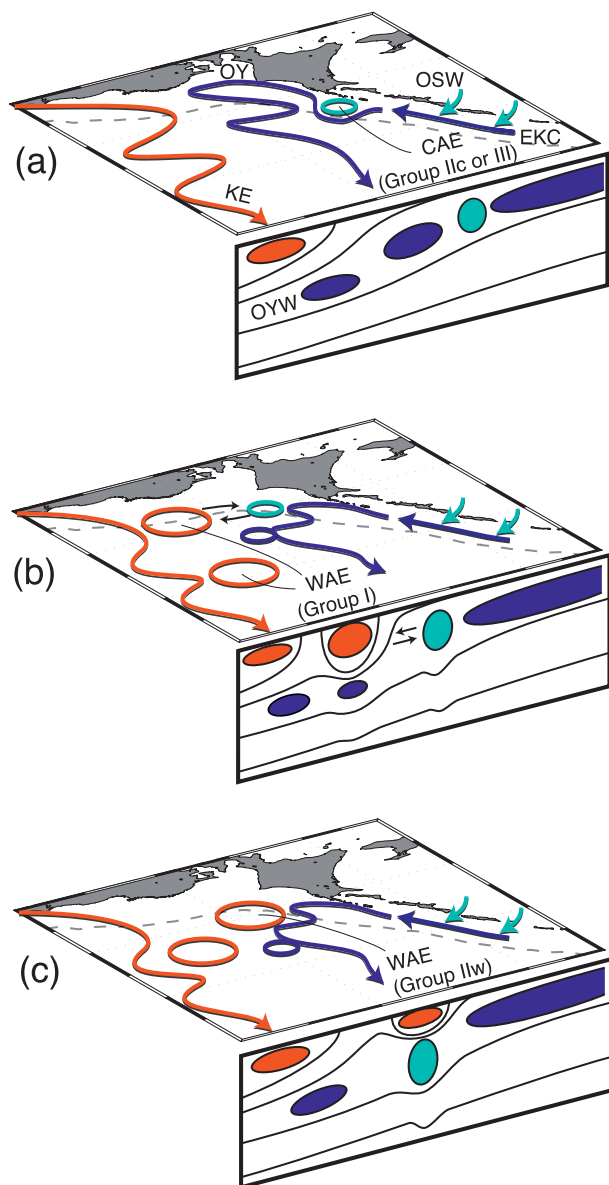


FIG. 15. Schematic diagram of the formation and evolution of WAE and CAE: (a) basic state, (b) formation of WAE and CAE, and (c) interaction and alignment of the eddies. In (a)–(c), the top part shows a plan view and the bottom part shows a cross section.

group I eddies corresponds to this type of double core, although in this case the upper core is generally much more prominent than the lower core.

The occurrence of cold and fresh anomalies on a horizontal plane at the same depth can be maintained by depression of an isopycnal surface, if the upper layer contains colder and fresher water than the lower layer. This condition is often satisfied in the western subarctic North Pacific. In addition, if the propagation speed of an eddy exceeds the swirling velocity at a certain depth,

then the core water is replaced by ambient water (Flierl 1981) that is depressed downward to form a cold and fresh anomaly. Thus, for some warm eddies that propagate poleward to the subarctic area, ambient water may appear in a deep layer as cold and freshwater anomalies.

Although the above process may explain some minor cases of double-core structure, it is not applicable to strongly developed cases for which a water mass shows cold and fresh anomalies on an isopycnal surface. We suggest that this full double-core structure is caused by interaction between warm and cold water masses, both of which have low potential vorticity. Two types of interactions are suggested in this regard: between the Kuroshio Extension and a cold water mass and between warm and cold anticyclonic eddies. The former type of interaction is generally recognized as shedding of a warm eddy from the Kuroshio Extension. Mooring observations indicate that downstream-propagating meanders with horizontal scales of 220–380 km have characteristics consistent with baroclinic instability waves (Itoh and Sugimoto 2008), which are considered to play a part in the above interaction. Another important factor is the moderately cold and fresh Oyashio water in the intermediate layer, as seen in the θ and S minima in Figs. 7d,e, respectively. Although Q values in eddy profiles are not significantly lower than those of the climatology at denser than $26.50\sigma_\theta$ (Fig. 11a), this does not necessarily indicate that potential vorticity (including relative vorticity) was not low: we presume that a relatively thick cold water mass is compressed as a consequence of interaction with a thick and intense warm water mass of the Kuroshio Extension. In such a case, the cold water mass obtains negative relative vorticity (anticyclonic rotation) and potential vorticity is maintained at low levels.

The relevance of instability to potential vorticity has also been reported by Kouketsu and Yasuda (2008), who performed a linear stability analysis, revealing that the low-potential-vorticity intermediate layer, generated by intrusion of the Oyashio, has a generally positive effect on the growth rate of the disturbance at a length scale of ~ 200 km. Given that Q values decrease with decreasing salinity (Fig. 12), we suggest that meanders of the Kuroshio Extension are susceptible to interaction with cold and freshwater masses, thereby forming warm eddies.

Interaction between warm and cold anticyclonic eddies (shown by arrows in Fig. 15b) may play an important role in terms of eddy persistence and northeastward propagation. A supply of low-potential-vorticity water is crucial for the maintenance of anticyclonic swirling velocity, especially in the subarctic area, where interaction with other warm eddies is less likely than in the southern area. The coupling of warm and cold eddies is interpreted as alignment, which is defined as the coalescence

of two eddies in different layers (Polvani 1991). The fact that the radii of observed eddies are larger than the radius of Rossby deformation (Chelton et al. 1998) is consistent with the conditions thought to be necessary for alignment to occur.

Another point to note is the deep penetration of the eddy structure. As shown in Fig. 14, the structure of some eddies clearly extends deeper than 2000 dbar. Because the planetary β effect drives eddies westward, those with deep penetration near a western boundary inevitably interact with the bottom slope, which may explain the eastward shift in eddy axes in deep layers. An eastward tilt of the eddy axis with respect to depth causes net poleward heat transport due to the correlation of temperature and velocity (Roemmich and Gilson 2001). In the case of warm eddies such as eddy IIw-04 (Fig. 14), the northward transport of positive temperature anomaly results in the northward propagation of the gravitational center of the warm core, thereby producing the apparent northward movement of the eddy. This phenomenon is consistent with the results of a previous numerical study that examined eddy–slope interactions (Itoh and Sugimoto 2001), in that an isolated anticyclonic eddy may propagate northward along the western boundary of the ocean. Quasi-steady propagation is possible if the steep slope of JT and KTT exert the image effect (Itoh and Sugimoto 2001) or a low pressure anomaly is formed near the slope below the upper-layer warm core, as a part of “heton” (Hogg and Stommel 1985). However, it needs further investigations to confirm the availability of the above processes.

Although anticyclonic warm eddies generally occur from other western boundary currents in the global ocean, none has a double-core structure or shows long-term poleward propagation, in contrast to that observed in the western North Pacific. We suggest that the occurrence of cold anticyclonic eddies is partly responsible for this behavior. Although the warm and saline upper core causes significant poleward heat and salinity transport in the upper layer, possibly influencing heat transport to the atmosphere, the cold and fresh lower core that is distributed at around $26.7\sigma_\theta$ and that originated from the Sea of Okhotsk may contribute to the Oyashio.

Acknowledgments. S. Itoh was financially supported by the Japanese Ministry of Education, Culture, Sports, Science and Technology [KAKENHI; Grand-in-Aid for Young Scientists (B) 21740340].

REFERENCES

- Argo Science Team, 2001: The global array of profiling floats. *Observing the Oceans in the 21st Century*, GODAE Project Office, 248–258.
- Boyer, T. P., and Coauthors, 2006: *World Ocean Database 2005*. NOAA Atlas NESDIS 60, 190 pp.
- Byrne, D. A., A. L. Gordon, and W. F. Haxby, 1995: Agulhas eddies: A synoptic view using Geosat ERM data. *J. Phys. Oceanogr.*, **25**, 902–917.
- Chelton, D. B., R. A. deSzoeke, M. G. Schlax, K. El Naggar, and N. Siwertz, 1998: Geographical variability of the first baroclinic Rossby radius of deformation. *J. Phys. Oceanogr.*, **28**, 433–460.
- , M. G. Schlax, R. M. Samelson, and R. A. de Szoeke, 2007: Global observations of large oceanic eddies. *Geophys. Res. Lett.*, **34**, L15606, doi:10.1029/2007GL030812.
- Conkright, M. E., R. A. Locarnini, H. E. Garcia, T. D. O'Brien, T. P. Boyer, C. Stephens, and J. I. Antonov, 2002: *World Ocean Atlas 2001: Objective Analyses, Data Statistics, and Figures, CD-ROM Documentation*. National Oceanographic Data Center, 17 pp.
- Curry, R. G., 2001: HydroBase 2—A database of hydrographic profiles and tools for climatological analysis. 81 pp.
- Elliott, B. A., 1982: Anticyclonic rings in the Gulf of Mexico. *J. Phys. Oceanogr.*, **12**, 1292–1309.
- Flierl, G. R., 1981: Particle motions in large-amplitude wave fields. *Geophys. Astrophys. Fluid Dyn.*, **18**, 39–74.
- Fritsch, F. N., and R. E. Carlson, 1980: Monotone piecewise cubic interpolation. *SIAM J. Numer. Anal.*, **17**, 238–246.
- Gordon, A. L., 1985: Indian-Atlantic transfer of thermocline water at the Agulhas Retroflexion. *Science*, **227**, 1030–1033.
- Hogg, N. G., and H. M. Stommel, 1985: The heton, an elementary interaction between discrete baroclinic geostrophic vortices, and its implications concerning eddy heat-flow. *Proc. Roy. Soc. London*, **397A**, 1–20.
- Itoh, S., and T. Sugimoto, 2001: Numerical experiments on the movement of a warm-core ring with the bottom slope of a western boundary. *J. Geophys. Res.*, **106**, 26 851–26 862.
- , and —, 2008: Current variability of the Kuroshio near the separation point from the western boundary. *J. Geophys. Res.*, **113**, C11020, doi:10.1029/2007JC004682.
- , and I. Yasuda, 2010: Characteristics of mesoscale eddies in the Kuroshio–Oyashio Extension Region detected from the distribution of the sea surface height anomaly. *J. Phys. Oceanogr.*, **40**, 1018–1034.
- Kawai, H., 1969: Statistical estimation of isotherms indicative of Kuroshio axis. *Deep-Sea Res.*, **16**, 109–115.
- , 1972: Hydrography of the Kuroshio Extension. *Kuroshio: Its Physical Aspects*, H. Stommel and K. Yoshida, Eds., University of Tokyo Press, 235–352.
- Kitano, K., 1975: Some properties of warm eddies generated in the confluence zone of the Kuroshio and Oyashio currents. *J. Phys. Oceanogr.*, **5**, 245–252.
- Kouketsu, S., and I. Yasuda, 2008: Unstable frontal waves along the Kuroshio Extension with low-potential vorticity Intermediate Oyashio Water. *J. Phys. Oceanogr.*, **38**, 2308–2321.
- Lobanov, V. B., and N. V. Bulatov, 1993: Physical structure and behavior of the Kuril eddies. *Proc. Nemuro Workshop on Western Subarctic Circulation*, Nemuro, Japan, North Pacific Marine Science Organization (PICES), 27–30.
- Nilsson, C. S., and G. R. Cresswell, 1980: The formation and evolution of East Australian current warm-core eddies. *Prog. Oceanogr.*, **9**, 133–183.
- Olson, D. B., 1991: Rings in the ocean. *Annu. Rev. Earth Planet. Sci.*, **19**, 283–311.
- , G. P. Podesta, R. H. Evans, and O. B. Brown, 1988: Temporal variations in the separation of Brazil and Malvinas Currents. *Deep-Sea Res.*, **35**, 1971–1990.

- , R. A. Fine, and A. L. Gordon, 1992: Convective modifications of water masses in the Agulhas. *Deep-Sea Res.*, **39**, S163–S181.
- Polvani, L. M., 1991: Two-layer geostrophic vortex dynamics. Part 2. Alignment and two-layer V-states. *J. Fluid Mech.*, **225**, 241–270.
- Qiu, B., P. Hacker, S. M. Chen, K. A. Donohue, D. R. Watts, H. Mitsudera, N. G. Hogg, and S. R. Jayne, 2006: Observations of the subtropical mode water evolution from the Kuroshio Extension System Study. *J. Phys. Oceanogr.*, **36**, 457–473.
- Richardson, P. L., 1983: Gulf Stream rings. *Eddies in Marine Science*, A. R. Robinson, Ed., Springer-Verlag, 17–45.
- Ring Group, 1981: Gulf-Stream cold-core rings—Their physics, chemistry, and biology. *Science*, **212**, 1091–1100.
- Rio, M.-H., and F. Hernandez, 2004: A mean dynamic topography computed over the world ocean from altimetry, in situ measurements, and a geoid model. *J. Geophys. Res.*, **109**, C12032, doi:10.1029/2003JC002226.
- Roemmich, D., and J. Gilson, 2001: Eddy transport of heat and thermocline waters in the North Pacific: A key to interannual/decadal climate variability? *J. Phys. Oceanogr.*, **31**, 675–687.
- Rogachev, K. A., 2000: Recent variability in the Pacific western subarctic boundary currents and Sea of Okhotsk. *Prog. Oceanogr.*, **47**, 299–336.
- Shimizu, Y., I. Yasuda, and S. Ito, 2001: Distribution and circulation of the coastal Oyashio intrusion. *J. Phys. Oceanogr.*, **31**, 1561–1578.
- Suga, T., K. Hanawa, and Y. Toba, 1989: Sub-tropical mode water in the 137°E section. *J. Phys. Oceanogr.*, **19**, 1605–1618.
- Talley, L. D., 1988: Potential vorticity distribution in the North Pacific. *J. Phys. Oceanogr.*, **18**, 89–106.
- , Y. Nagata, M. Fujimura, T. Iwao, T. Kono, D. Inagake, M. Hirai, and K. Okuda, 1995: North Pacific Intermediate Water in the Kuroshio/Oyashio mixed water region. *J. Phys. Oceanogr.*, **25**, 475–501.
- Ueno, H., and I. Yasuda, 2000: Distribution and formation of the mesothermal structure (temperature inversions) in the North Pacific subarctic region. *J. Geophys. Res.*, **105**, 16 885–16 897.
- Yasuda, I., K. Okuda, and M. Hirai, 1992: Evolution of a Kuroshio warm-core ring – variability of the hydrographic structure. *Deep-Sea Res.*, **39**, S131–S161.
- , —, and Y. Shimizu, 1996: Distribution and modification of North Pacific Intermediate Water in the Kuroshio-Oyashio interfrontal zone. *J. Phys. Oceanogr.*, **26**, 448–465.
- , and Coauthors, 2000: Cold-core anticyclonic eddies south of the Bussol' Strait in the northwestern subarctic Pacific. *J. Phys. Oceanogr.*, **30**, 1137–1157.